Radial Profile Estimation of Electron Density in a Linear Plasma Device NUMBER Using a Single Line-of-Sight Signal*)

Minami SUGIMOTO, Atsushi OKAMOTO, Takaaki FUJITA, Hideki ARIMOTO, Shunya HIGUCHI and Konan YAGASAKI

Graduate School of Engineering, Nagoya University, Furo-cho, Chikusa-ku, Nagoya 464-8603, Japan

(Received 30 November 2020 / Accepted 12 January 2021)

In this paper, a method for estimating the radial profile of electron density n_e using a single line-of-sight signal by the He I line intensity ratio method is proposed. By applying this method to cylindrical helium plasma, in which electron temperature was almost uniform and density was uniform in the center, we tried to estimate the parameters representing spatial distribution. It was confirmed that a good distribution estimation result could be obtained by considering the sensitivity factor, the rate at which the line intensity ratio changes as the parameters change, during optimization. Two methods of considering a sensitivity factor are proposed: using the best combination of intensity ratios for analysis in terms of the sensitivity factor, and weighting the objective function using the sensitivity factor. The former method can be analyzed in short computational time, although its applicability is limited. The latter method can be used when it is not obvious which set of intensity ratios is best to use, although it takes more computational time compared with the former method. Both methods reproduce the parameter of a radial density profile.

Keywords: He I line intensity ratio, collisional radiative model, spatial distribution estimation, linear plasma device, parameter optimization

DOI: 10.1585/pfr.16.2401042

1. Introduction

Electron density n_e and temperature T_e are important parameters in plasmas, and they are measured by various methods. The He I line intensity ratio method that is a kind of spectroscopic diagnostics is often used to obtain n_e and T_e [1]. Since line intensity ratios are expressed in terms of population density, we can obtain n_e and T_e by comparing a measured line intensity ratio to the calculated population density. Typically, collisional radiative models are used for the calculation of population density using n_e and T_e.

To measure spatial distribution by the He I line intensity ratio method, local emission intensity is often reconstructed using multiple integrated intensities along lines of sight. If sufficient lines of sight are not available, reconstruction fails.

The linear plasma device NUMBER (Nagoya Univ. Magnetoplasma Basic Experiment) was primarily designed for the development of high-energy ion production methods for the simulation of alpha particles [2] and for a divertor plasma study [3]. In NUMBER, we measured He I emission lines at only one line of sight owing to the limitations of the port configuration. Although spatial distribution was measured using probes, it was desirable to easily measure spatial distribution by a non-contact method. Therefore, we propose a method for estimating spatial distribution using line-integrated emission intensities along only one line of sight. In this paper, a simple radial profile of electron density is estimated using single line-of-sight spectroscopic signals. Methods used for the calculation of intensity ratio and optimization of parameters are described in Section 2. The experimental setup is described in Section 3, followed by the results and discussion in Section 4. The paper is summarized in Section 5.

2. Method

Details of the calculation of the line-integrated intensity ratio and optimization of parameters are described in this section.

2.1 Calculation

Assuming the radial uniformity of a neutral particle density, the ratio of line-integrated emission intensity can be expressed as

$$\rho = \frac{\int I_{p\to q}(l)\mathrm{d}l}{\int I_{p'\to q'}(l)\mathrm{d}l} = \frac{\int A_{p\to q}\cdot n(p,\,l)\mathrm{d}l}{\int A_{p'\to q'}\cdot n(p',\,l)\mathrm{d}l}\,, \tag{1}$$

where $I_{p\to q}(l)$ is local emission intensity from level p to q, $A_{p\to q}$ is the spontaneous transition probability from p to q, and $n(p,\,l)$ is the local population density of level p at a distance l along the line of sight.

Local population density is calculated using the collisional radiative model for neutral helium [4, 5]. As for

author's e-mail: sugimoto.minami@b.mbox.nagoya-u.ac.jp

*) This article is based on the presentation at the 29th International Toki Conference on Plasma and Fusion Research (ITC29).

radiation trapping, the intensity of radiation field $I_{3^1\mathrm{P}}$ is introduced [6], where $I_{3^1\mathrm{P}}$ is a photo-excitation rate from 1^1S to 3^1P. The rate equation can be written as

$$\frac{\mathrm{d}n(p)}{\mathrm{d}t} = -\left\{\sum_{q\neq p} C_{p\to q}n_e + \sum_{q<p} A_{p\to q} + S_p n_\mathrm{e}\right\} n(p) + \sum_{q\neq p} C_{q\to p}n_e n(q) + \sum_{q>p} A_{q\to p}n(q) + \delta_{p,3^1\mathrm{P}} I_{3^1\mathrm{P}} n(1^1\mathrm{S}), \quad (2)$$

where $C_{p\to q}$ is the rate coefficient for electron impact transition (excitation/de-excitation) from p to q, S_p is the rate coefficient for electron impact ionization, and $\delta_{p,3^1\mathrm{P}}$ is Kronecker delta, which is 1 when $p = 3^1$P and 0 otherwise. Assuming quasi-steady-state approximation, except for the ground state, population density is calculated for ionizing plasma. Then, $n(p)$ is given as a function of n_e, T_e, and $I_{3^1\mathrm{P}}$.

To integrate population density along the line of sight, we assume the spatial distribution of n_e, T_e, and $I_{3^1\mathrm{P}}$. It is better that the function of the radial profile can be expressed using less parameters that reproduce real plasma. In this study, the following function is applied to the radial profile of n_e, using central electron density $n_{\mathrm{e}0}$ and the parameter r_1:

$$n_\mathrm{e}(r) = \begin{cases} n_{\mathrm{e}0} & (r \le r_1) \\ n_{\mathrm{e}0}\dfrac{(2r - 3r_1 + r_0)}{(r_0 - r_1)^3}(r - r_0)^2 & (r_1 \le r \le r_0). \end{cases} \quad (3)$$

The plasma edge r_0 is set to 90 mm based on probe measurements. T_e and $I_{3^1\mathrm{P}}$ are assumed to be uniform : $T_\mathrm{e}(r) = T_e$, $I_{3^1\mathrm{P}}(r) = I_{3^1\mathrm{P}}$.

With these assumptions, the integrated intensity ratio ρ is obtained by inputting the parameter $\mathbf{x} = (T_\mathrm{e}, n_\mathrm{e}, r_1, I_{3^1\mathrm{P}})$ into the model. The best value of $\mathbf{x}$ is determined by optimization.

2.2 Optimization

The abovementioned parameters are updated so that the objective function is minimized. In this study, two objective functions were used for optimization. First is the simple function

$$F_1(\mathbf{x}) = \sqrt{\sum_i \left(\frac{\rho_i^{\mathrm{exp}} - \rho_i^{\mathrm{cal}}}{\sigma_i^{\mathrm{exp}}}\right)^2}, \quad (4)$$

where i is the index of the intensity ratio, ρ_i^{cal} is the calculation value, ρ_i^{exp} is the mean of the experimental data, and σ_i^{exp} is the standard deviation of the experimental data. The second function $F_2(\mathbf{x})$ is weighted using a sensitivity factor.

$$F_2(\mathbf{x}) = \sqrt{\sum_i \left(\frac{\sum_n \sum_m S_{\rho_n, x_m}}{\sum_j S_{\rho_i, x_j}} \left(\frac{\rho_i^{\mathrm{exp}} - \rho_i^{\mathrm{cal}}}{\sigma_i^{\mathrm{exp}}}\right)^2\right)}. \quad (5)$$

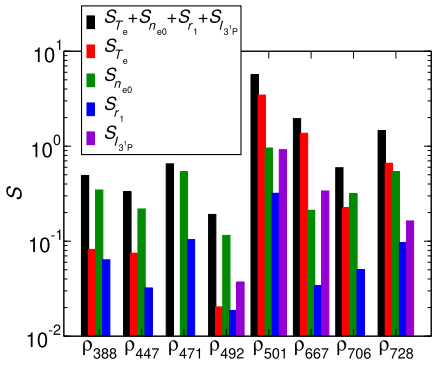

Fig. 1 Values of sensitivity factor for normalized intensity ratios: ρ_λ stands for the ratio of line intensity at λ [nm] to that at 587 nm. The values were calculated with the value of each parameter as $T_\mathrm{e} = 5$ eV, $n_{\mathrm{e}0} = 1 \times 10^{18}$ m^{-3}, $r_1 = 45$ mm, and $I_{3^1\mathrm{P}} = 100$ s^{-1}.

Herein, S_{ρ_i, x_j} is the sensitivity factor of the ith intensity ratio ρ_i for jth parameter x_j and is defined by

$$S_{\rho_i, x_j} = \left|\frac{\partial \rho_i}{\partial x_j} \cdot \frac{x_j}{\rho_i}\right|. \quad (6)$$

The sensitivity factor is calculated using central difference in the parameter space. Intensity ratios $\rho_i(\mathbf{x})$ are calculated using the collisional radiative model and by changing the value of each parameter by $\pm 1\%$.

An example of the values of sensitivity factors are shown in Fig. 1. In this figure, the sum of the sensitivity factor $\sum_j S_{\rho_i, x_j}$, for each intensity ratio is shown, as well as the sensitivity for the specific parameter S_{ρ_i, x_j}. The highest sensitivity factor is for ρ_{501} and the lowest is for ρ_{492}. For these two intensity ratios, the difference is about an order of magnitude. Furthermore, a breakdown of the sensitivity of ρ_{501} shows that the sensitivity for T_e, $S_{\rho_{501}, T_\mathrm{e}}$ is about an order of magnitude greater than that for r_1, S_{ρ_{501}, r_1}. This means that the line intensity ratio changes by the same magnitude when T_e changes by 1% and when r_1 changes by 10%. The second and third largest (ρ_{667} and ρ_{728}) have similar parameter dependence. There are intensity ratios, which have no sensitivity to T_e and have relatively higher sensitivity to r_1, such as ρ_{471}. However, because the absolute value of the sensitivity factor is small, it is difficult for this ratio to affect an unweighted objective function, F_1. By weighting as F_2, all intensity ratios will contribute equally to the objective function.

The Nelder-Mead method [7] was used as the optimization algorithm. The code implemented in the python package SciPy [8] was adopted. This algorithm does not require a derivative of the objective function. First, this algorithm calculates the objective function from $\mathbf{x}_1$ to $\mathbf{x}_{n+1}$, where n is the dimension of $\mathbf{x}$. The initial value is $\mathbf{x}_1 = (T_\mathrm{e} = 5\,\mathrm{eV}, n_{\mathrm{e}0} = 1 \times 10^{18}\,\mathrm{m}^{-3}, r_1 = 45\,\mathrm{mm}, I_{3^1\mathrm{P}} = 100\,\mathrm{s}^{-1})$, $\mathbf{x}_i = 1.05 \times \mathbf{x}_{i-1}$. Then, by applying four operations (reflection, expansion, contraction, and compression), the maximum objective function among them is up-

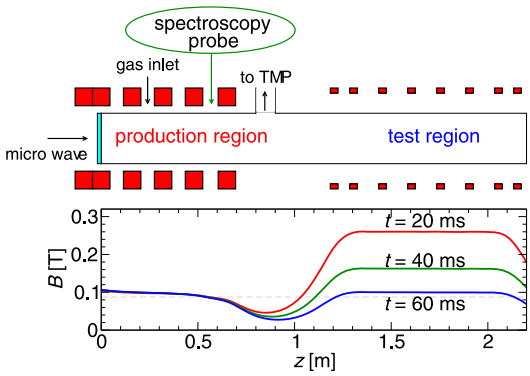

Fig. 2 Schematic of NUMBER and magnetic field strength at $r = 0$ mm.

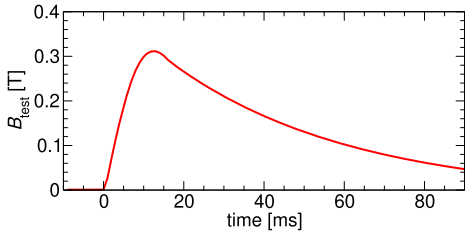

Fig. 3 Time evolution of the strength of the magnetic field in the test region ($z = 1.53$ m).

dated. By repeatedly updating $\mathbf{x}$, we obtain the optimized parameters $\mathbf{x}$, where the objective function is a minimum. The stopping condition is that the difference of the objective function for all pairs in $\mathbf{x}_1, \mathbf{x}_2, \ldots, \mathbf{x}_{n+1}$ is less than 10^{-4}.

3. Experimental Setup

Experiments were performed using a linear plasma device NUMBER [2]. The length of NUMBER is about 2 m and its diameter is 0.2 m. As shown in Fig. 2, the device consists of a production region (0 m $< z <$ 0.7 m) and a test region (1.1 m $< z <$ 2 m), where z is a distance along the cylindrical axis. By injecting a microwave (2.45 GHz, 6 kW) from the window at $z = 0$ m, the cylindrical plasma is generated by electron cyclotron resonance in the production region. By applying a pulsed magnetic field to the test region shown in Fig. 3, the plasma is transported from the production region to the test region. When the strength of the magnetic field in the test region is larger than approximately 0.1 T, the electron density is significantly higher in both the production region and test region compared to the low magnetic field in the test region [2, 3].

He I line emissions were measured. The line of sight was in the radial direction at $z = 0.57$ m. A multichannel spectrometer was used to obtain a spectrum in the wavelength range of 343 - 828 nm. Then, nine line emissions were identified, which are shown in Table 1. The wavelength resolution was ~ 0.3 nm. The spectrometer was calibrated for sensitivity by using a xenon lamp as a standard light source. The uncertainty of this light source is 5% - 10%, depending on the wavelength. The transparency of the measurement window was not considered. The time resolution of the measurements was 2 ms and the spectra were taken for 100 ms. These measurements were carried out for 23 shots with the same conditions. The mean value and standard deviation of line intensity among the shots were used for analysis. The standard deviation was 1% - 20% of the mean of intensity, as shown in Table 1. The uncertainty due to photometric calibration are not included.

Table 1 He I emission lines observed in the experiment.

Wavelength [nm]	Transition	Intensity*
388.86	$2^3S - 3^3P$	$(2.5 \pm 0.2) \times 10^{11}$
447.14	$2^3P - 4^3D$	$(1.58 \pm 0.08) \times 10^{11}$
471.31	$2^3P - 4^3S$	$(3.2 \pm 0.5) \times 10^{10}$
492.19	$2^1P - 4^1D$	$(3.7 \pm 0.3) \times 10^{10}$
501.56	$2^1S - 3^1P$	$(9.4 \pm 0.3) \times 10^{10}$
587.56	$2^3P - 3^3D$	$(1.48 \pm 0.02) \times 10^{12}$
667.81	$2^1P - 3^1D$	$(3.49 \pm 0.06) \times 10^{11}$
706.51	$2^3P - 3^3S$	$(5.12 \pm 0.07) \times 10^{11}$
728.13	$2^1P - 3^1S$	$(9.7 \pm 0.5) \times 10^{10}$

$*$ at $t = 18$ - 20 ms, unit is photon/cm^2/sr

To evaluate the estimation results, the radial profile was also measured using a single probe. The sweep frequency of the probe voltage was 250 Hz and the radial position of the probe was changed by 10 mm for each shot.

4. Results and Discussion

In this study, two sets of line intensity ratios were used for analysis. Set (a) is ratios for all line intensities normalized by I_{587}. Set (b) is four ratios consisting of I_{471}/I_{388}, I_{587}/I_{471}, I_{706}/I_{501}, and I_{706}/I_{587}. Set (b) is an empirically successful ratios, in which there are few intensity ratios with extremely high sensitivity factor for T_e and the sensitivity is reasonably high for all parameters. The sensitivity factors for intensity ratios in Set (b) are shown in Fig. 4.

From the combination of two sets of intensity ratios and two objective functions, we applied three patterns: (A) F_1 and Set (a), (B) F_1 and Set (b), and (C) F_2 and Set (a). The results for each pattern and the values obtained using the probe are shown in Fig. 5. In Fig. 5, the high-density phase is observed at time $t = 10$ - 45 ms. Transition to the high-density phase is so rapid compared with time resolutions of both probe and spectroscopy measurements that there is deviation in n_{e0} between these measurements at $t \simeq 8$ ms. The number of iterations for the Nelder-Mead method was about 200 times for each time step. The calculation time for 50 points of time was 1 hour for F_1 and about 7 hours for F_2 with a standard personal computer.

First, we discuss Pattern (A). In this pattern, good rough estimates were obtained for high sensitivity param-

eters T_e and n_e. However, compared to probe measurements, the value of T_e tends to be slightly lower and the value of n_e tends to be higher. The less sensitive parameter, r_1, cannot be estimated well as it frequently stays at the upper limit. In the objective function F_1, without weighting, the sensitivity of the objective function to r_1 is so small that the objective function hardly changes when r_1 changes significantly. If there is a large difference in sensitivity factor among the intensity ratios used for estimation, the residual squares for the intensity ratios with high sensitivity factors, such as ρ_{501} would be minimized in the optimization. As a result, the other residual squares do not become sufficiently small, making it difficult to optimize the parameters.

In contrast, Pattern (B) returns a better solution for r_1. The reason for this success is the choice of the intensity ratios. Comparing Fig. 1 and Fig. 4, in Set (a) there are intensity ratios with high sensitivity in T_e, whereas, in Set (b) only one intensity ratio ($\rho_{706/501}$) has a sensitivity factor over one for T_e. In addition, the other three intensity ratios can be considered as a combination of approximately equal contributions to the objective function because the sums of the sensitivity factors are the same order of magnitude. As a result, all residual squares are sufficiently small.

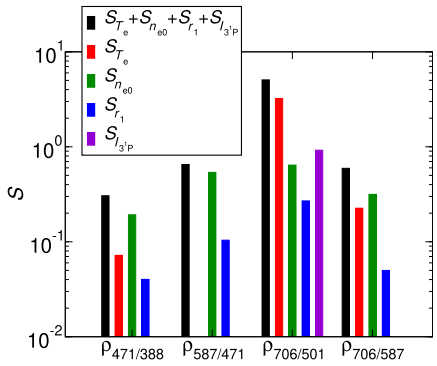

Fig. 4 Values of sensitivity factor for intensity ratios in Set (b). The values were calculated with the value of each parameter as $T_e = 5\,\mathrm{eV}$, $n_{e0} = 1 \times 10^{18}\,\mathrm{m}^{-3}$, $r_1 = 45\,\mathrm{mm}$, and $I_{3^1P} = 100\,\mathrm{s}^{-1}$.

Less calculation time is required when using objective function F_1. Therefore, Pattern (B) is one of the best method for estimating the radial density profile of this plasma. However, the selection of a suitable intensity ratio is empirical and will be difficult for a large number of parameters and emission lines.

This difficulty can be reduced by weighting, although it takes time to calculate. Pattern (C) with F_2 returns better results for parameters than Pattern (A), including r_1. This result suggests that the weighted objective function F_2 is effective. This weighting decreases the contribution of intensity ratios with high sensitivity factors, such as ρ_{501}, to

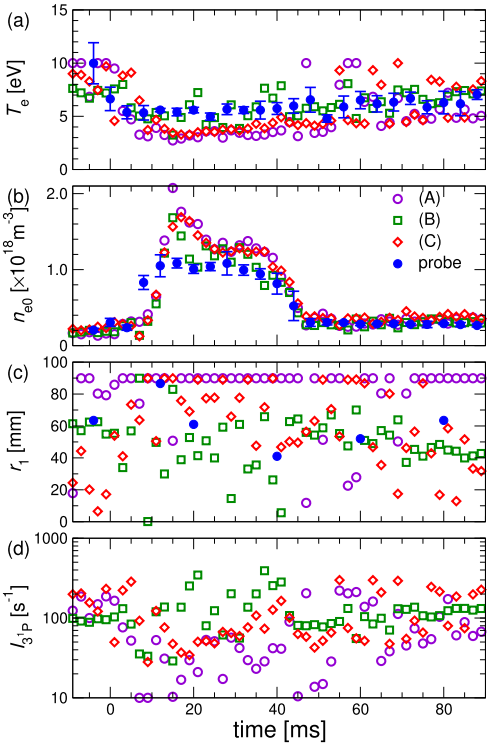

Fig. 5 Value of each parameter obtained by optimization with three patterns (A) - (C) of the objective function. (a) Electron temperature, (b) center electron density, (c) profile parameter, and (d) photo-excitation rate.

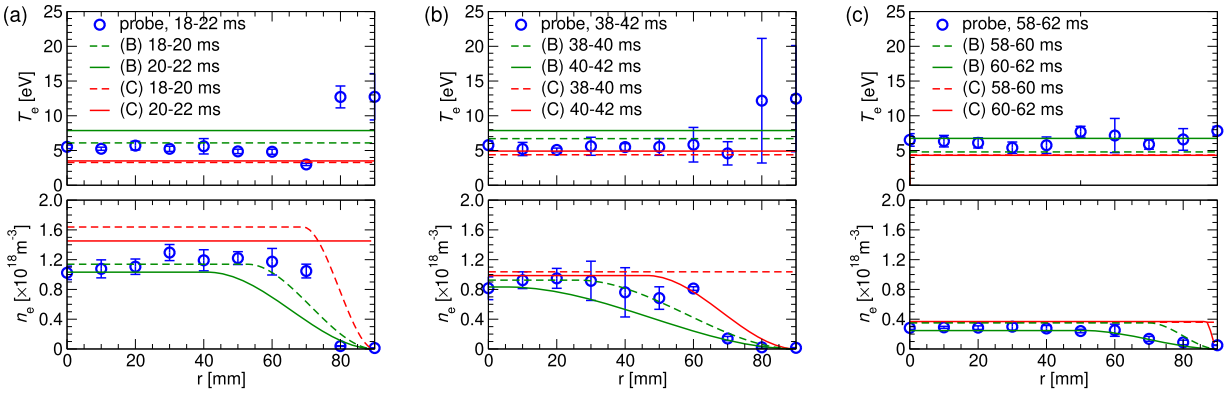

Fig. 6 Radial profile of T_e and n_e in patterns (B) and (C) at (a) $t = 20\,\mathrm{ms}$, (b) $t = 40\,\mathrm{ms}$, and (c) $t = 60\,\mathrm{ms}$.

the objective function. Then, the residual squares of other intensity ratios are reduced. As a result, even when all eight intensity ratios were used, the results were close to those of Pattern (B).

The radial profiles estimated in patterns (B) and (C) are shown in Fig. 6. Because of the difference in the time windows of the probe and spectroscopy measurements, the two results from spectroscopy are plotted for one probe data.

Three time slices correspond to the high-density phase [3], marginally high-density phase, and the low-density phase. In particular, for Pattern(B), radial profiles of electron density are well reproduced for probe measurements in these time slices. Moreover, in Pattern (C), if r_1 does not stay at the upper limit the results roughly represent the actual n_e profile. The electron temperatures, which are assumed uniform, also match with the probe data in the core region ($n_e \geq n_{e0}/2$). In the high-density phase, Figs. 6 (a) and (b), the electron temperature at the edge ($n_e \leq n_{e0}/2$) is higher than that in the core region. Due to lower density in the edge, contribution of the higher temperature to line-integrated intensity is limited. Estimation of temperature profile as well as that for density remains our future work.

5. Summary

The radial profile of the electron density was estimated from a single line-of-sight signal using the He I line intensity ratio method. The target plasma was a cylindrical plasma, wherein the electron temperature is almost uniform and the density is flat in the center. By selecting suitable intensity ratios, the radial density profile was reproduced, as well as the center density and temperature. This is understood in terms of the sensitivity factors. A more general method, which can be used when the best set of intensity ratios to use is unknown, was also proposed. Although it takes time to calculate, we roughly optimized the parameters representing the spatial distribution by weighting the objective function with the sensitivity factor.

Acknowledgments

One of the authors (M.S.) appreciate Dr. Goto at the National Institute for Fusion Science for providing a collisional radiative model. A part of this research was supported by JSPS KAKENHI Grant Numbers JP19H01869, JP20H01883.

[1] B. Schweer *et al.*, J. Nucl. Mater. **196-198**, 174 (1992).
[2] D. Hamada *et al.*, Plasma Fusion Res. **13**, 3401044 (2018).
[3] H. Hachikubo *et al.*, Plasma Fusion Res. **15**, 2401042 (2020).
[4] T. Fujimoto, J. Quant. Spectrosc. Radiat. Transf. **21**, 439 (1979).
[5] M. Goto, J. Quant. Spectrosc. Radiat. Transf. **76**, 331 (2003).
[6] K. Sawada *et al.*, Plasma Fusion Res. **5**, 001 (2010).
[7] J.A. Nelder and R. Mead, Computer Journal **7**, 308 (1965).
[8] P. Virtanen *et al.*, Nature Methods **17**, 261 (2020).